NANO LETTERS
Letter
Cite This: Nano Lett. 2019, 19, 6665−6672
pubs.acs.org/NanoLett

# High-Energy-Density Rechargeable Mg Battery Enabled by a Displacement Reaction

Minglei Mao,[†,‡,§] Tao Gao,[†,§] Singyuk Hou,[†] Fei Wang,[†] Ji Chen,[†] Zengxi Wei,[‡] Xiulin Fan,[†] Xiao Ji,[†] Jianmin Ma,[‡] and Chunsheng Wang*[,†]

[†]Department of Chemical and Biomolecular Engineering, University of Maryland, College Park, Maryland 20742, United States
[‡]School of Physics and Electronics, Hunan University, Changsha 410082, China

Supporting Information

**ABSTRACT:** Because of its high theoretical volumetric capacity and dendrite-free stripping/plating of Mg, rechargeable magnesium batteries (RMBs) hold great promise for high energy density in consumer electronics. However, the lack of high-energy-density cathodes severely constrains their practical applications. Herein, for the first time, we report that a CuS cathode can fully reversibly work through a displacement reaction in CuS/Mg pouch cells at room temperature and provide a high capacity of ∼400 mA h/g in a MACC electrolyte, corresponding to the gravimetric and volumetric energy density of 608 W h/kg and1042 W h/L, respectively. Even after 80 cycles, CuS/Mg pouch cells can maintain a high capacity of 335 mA h/g. Detailed mechanistic studies reveal that CuS undergoes a displacement reaction route rather than a typical conversion mechanism. This work will provide a guide for more discovery of high-performance cathode candidates for RMBs.

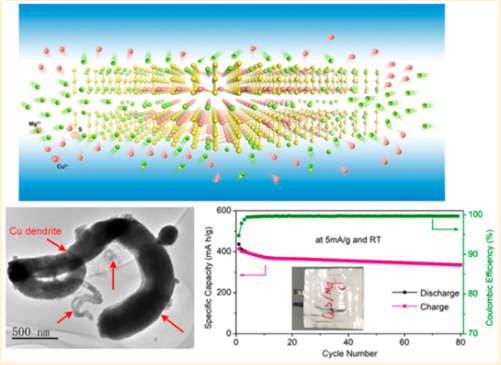


**KEYWORDS:** *Rechargeable Mg batteries, cathode materials, high energy density, displacement reaction, CuS*



Li ion batteries (LIBs) have been widely used in portable devices. However, with their energy density approaching the theoretical limit of intercalation chemistry,[1−3] rechargeable metal batteries, which can utilize the high capacity of metal anodes, are attracting more attention.[4−7] Compared to Li, Mg has a higher theoretical volumetric capacity (3833 mA h/cm$^3$ vs 2046 mA h/cm$^3$ for Li).[4,6,7] Besides its high abundance and lower reactivity in an ambient atmosphere,[8,9] a Mg metal anode can realize dendrite-free stripping/plating with close to 100% Coulombic efficiency in certain electrolytes,[10−12] which avoids the safety concern from an internal short circuit[13] and ensures long-duration cycling.[14] All of these merits make RMBs a promising candidate for consumer electronics application where the volumetric energy density and safety are priorities.[1,7]

Significant progress has been achieved in electrolytes, and several high-performance electrolytes, including Mg(AlCl$_2$BuEt)$_2$/THF,[15,16] MACC,[17−19] and APC,[9,16] have been developed. However, the development of RMBs is hindered by the lack of appropriate cathodes. The large charge/radius ratio of $Mg^{2+}$ results in a strong interaction between $Mg^{2+}$ and the host materials, which leads to sluggish kinetics and a low degree of magnesiation for most cathode materials.[4,6,7,20] The Chevrel phase ($Mo_6S_8$ or $Mo_6Se_8$) is still the most successful cathode that can work reversibly in a nonaqueous system at room temperature (RT).[21] However, because of its low voltage (1.2 V) and capacity (120 mA h/g), $Mo_6S_8$/Mg batteries can provide an energy density of only 140 W h/kg. Other intercalation cathodes, including spinel,[20,22−28] layered,[28−32] and polyanion materials,[33−35] can be reversibly intercalated by $Mg^{2+}$, but only at elevated temperature. Besides the intercalation cathodes, Mg/$I_2$,[36] Mg/$O_2$,[37−39] and especially Mg/S batteries[40−43] are also investigated because of their high potential capacities, but their reversibility needs to be further improved for practical application. To enhance the cycling stability of the sulfur cathode, metal sulfides have been investigated as potential Mg battery cathodes.[20,27,29]

CuS, as a typical transition-metal sulfide, can provide a high theoretical capacity of 560 mA h/g.[44,45] Its electrochemical activity through a conversion reaction mechanism for Mg batteries was first demonstrated by Nazar et al. at high temperature (150 °C).[46] Very recently, Mai's group further confirmed that CuS can provide 164 mA h/g at 55 °C at a low Coulombic efficiency of 68% because of a severe parasitic reaction with the current collector and the dissolution of CuS.[47] When the temperature decreases to 25 °C, the capacity of their CuS is reduced to less than 80 mA h/g and can be discharged/charged only for 20 cycles. It is believed that $Mg^{2+}$ "insertion/extraction" in CuS experiences a conversion reaction that has to break and rebuild the bond and results in a large overpotential and inferior kinetics[48,49] and thus low capacities at 25 °C. Besides, limited by the test cell, their CuS can be charged to only

Received: July 19, 2019
Revised: August 19, 2019
Published: August 21, 2019




DOI: 10.1021/acs.nanolett.9b02963
Nano Lett. 2019, 19, 6665−6672

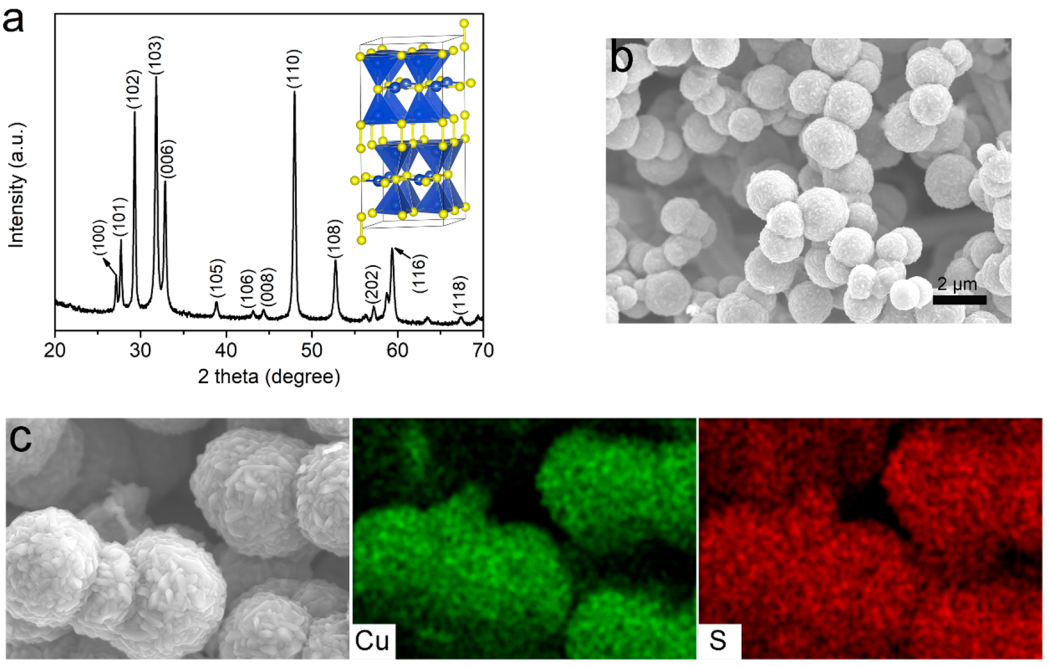


**Figure 1.** (a) Powder XRD pattern of the CuS microspheres sample is well matched with the standard card of JCPDS no. 06-0464. The inset is the structure of covellite CuS. Blue and yellow balls represent copper and sulfur atoms, respectively. (b) Low-resolution SEM and (c) energy-dispersive spectroscopy (EDS) mapping images of CuS microspheres.

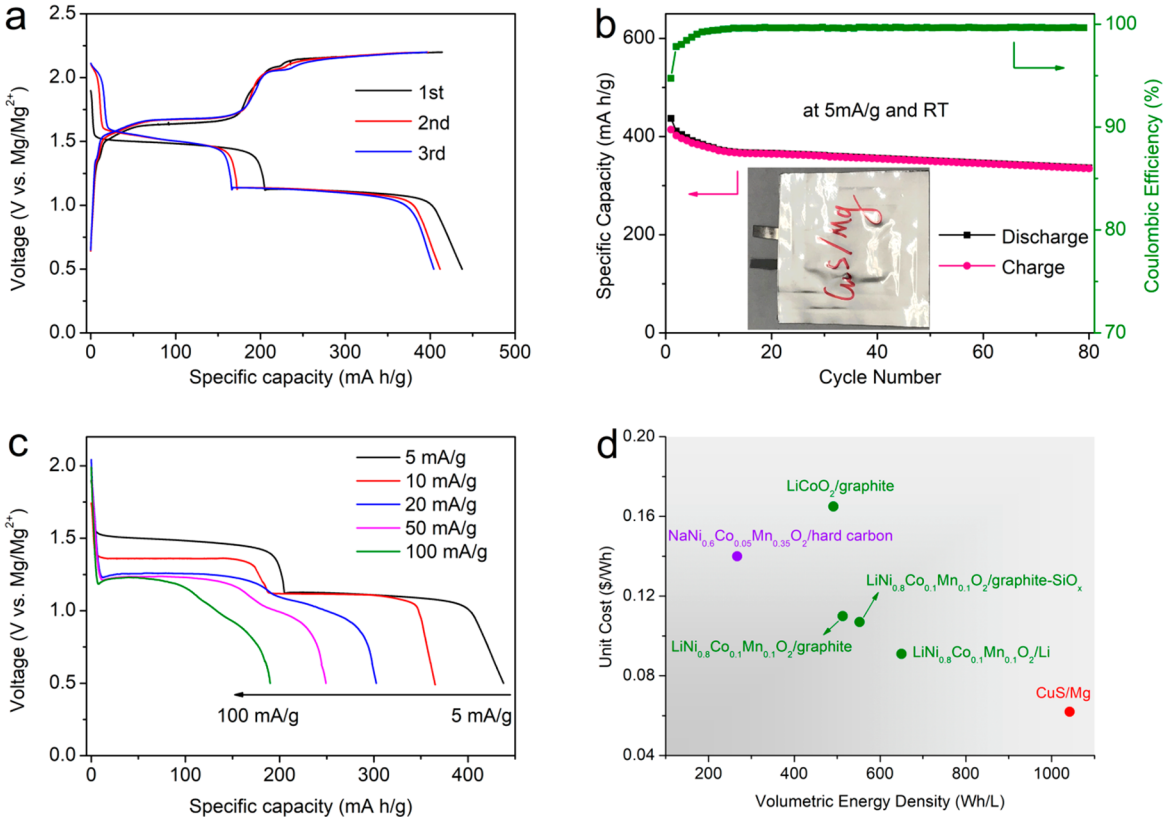


**Figure 2.** Electrochemistry of CuS microspheres with a MACC electrolyte and a Mg negative electrode using a pouch cell between 0.5 and 2.2 V at RT. (a) Discharge/charge curves of the first three cycles at 5 mA/g. (b) Cycling performance and Coulombic efficiency (CE) of the first 80 cycles at 5 mA/g. The inset is the pouch cell configuration. (c) Current density dependence of the discharge curve of CuS/Mg pouch cells. (d) Volumetric energy density versus unit cost of lithium ion batteries, sodium ion batteries, and rechargeable Mg batteries.

1.9 V vs $Mg/Mg^{2+}$ and does not accomplish complete reversibility of the CuS cathode, thus only ~14% of the theoretical capacity is achieved.

Herein, we, for the first time, demonstrate that CuS secondary microspheres assembled with primary CuS nanoparticles can fully reversibly work in pouch cells at RT through the



DOI: 10.1021/acs.nanolett.9b02963
*Nano Lett.* 2019, 19, 6665−6672

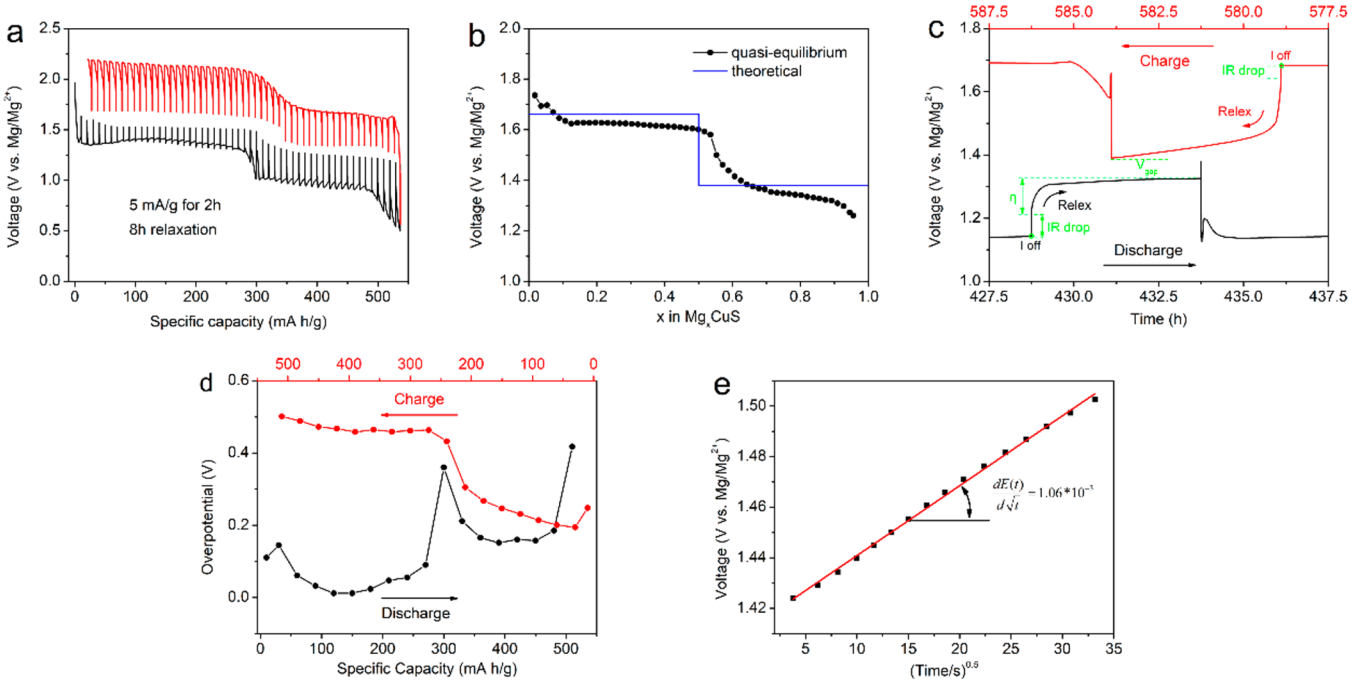


**Figure 3.** (a) Quasi-equilibrium voltage profile of the CuS/Mg system obtained from GITT. The cells were allowed to relax for 8 h after every 2 h of discharging or charging at 5 mA/g and RT. (b) Comparison of an experimental (black) and theoretical (blue) equilibrium voltage curve for CuS, after excluding the overpotential in the Mg negative electrode. (c) Close-up view of the GITT curve. The IR drop, reaction overpotential ($\eta$), and the remaining voltage difference after relaxation ($V_{gap}$) are marked to show the components that contribute to the voltage gap during cycling. (d) Absolute value of the voltage difference (IR+$\eta$) for the system with current on and after 8 h of relaxation for the discharging and charging process. (e) Representation of the transient voltage of the galvanostatic pulse as a function of the square root of the time for CuS. The red dashed line is the linear fitting, and the slope of the linear fitting is presented in the plot.

displacement reaction. The CuS/Mg pouch cell can achieve a high reversible capacity of ~400 mA h/g (~71% of the theoretical capacity) between 0.5 and 2.2 V for the first three cycles, corresponding to a volumetric energy density of ~1042 W h/L (more than twice that of the $LiCoO_2$/graphite pouch cell: 491 W h/L)[1−3] and a gravimetric energy density of 608 W h/kg. After 80 cycles, the CuS/Mg pouch cell is able to provide a capacity of ~335 mA h/g at 1.52 V, corresponding to the volumetric energy density of ~872 W h/L, much higher than that of Li−$O_2$ and Zn−$O_2$ batteries. Through mechanistic and kinetics investigations, we demonstrate that CuS undergoes a displacement reaction, and the fast diffusion of Cu favors the fast magnesiation and demagnesiation of CuS.

CuS was prepared by a modified hydrothermal method.[50] The phase of CuS microspheres is confirmed with powder X-ray diffraction (XRD). The characterized peaks match well with the standard card of JCPDS no. 06-0464 (Figure 1a), with the *P*63/*mmc* space group, consistent with previous reports.[50] SEM images show that the CuS secondary microspheres have a diameter of 2 to 3 $\mu$m (Figure 1b), which are assembled by primary nanoparticles (~200 nm) (Figure 1c). This configuration is important because the kinetics of magnesiation is limited by solid-phase diffusion.[9,22] The short ionic diffusion length provided by the primary nanoparticles should alleviate the resistance against magnesium ion diffusion in the solid phase and improve the electrode kinetics. The secondary particles have a size comparable to that of commercial $LiFePO_4$ particles,[51,52] which enables the high stacking density essential to achieving a reasonable volumetric energy density in practical application and reduces the side reaction of CuS with electrolytes.

The electrochemical performance of CuS/Mg pouch cells was examined with MACC as the electrolyte and Mg foil as the negative electrode at RT (Figure 2). A molybdenum grid is used as the current collector, which is stable in MACC electrolyte until 2.8 V (Figure S1). The discharge/charge curves of the first three cycles are shown in Figure 2a. The first discharge ($Mg^{2+}$ insertion) capacity reaches ~430 mA h/g, with two plateaus at 1.4 and 1.15 V, corresponding to 76.8% of the theoretical capacity of CuS with two electrons transferred (~560 mA h/g). The first plateau at ~1.4 V delivers a capacity of ~203 mA h/g, corresponding to 0.36 $Mg^{2+}$ transfer, and the second plateau at ~1.15 V achieves a capacity of 227 mA h/g, corresponding to 0.41 $Mg^{2+}$ transfer. When recharged to 2.2 V, two plateau of ~1.64 and 2.1 V can be clearly observed, with 96% of inserted $Mg^{2+}$ extracted (413 mA h/g). In the following cycling, both discharge and charge curves almost overlap, indicating a reversible reaction process (Figure 2a). The overpotential between discharge and charge processes is ~0.4 V (after excluding the overpotential of ~0.1 V in the Mg negative electrode (Figure S2)), which is much lower than for many cathode materials for RMBs[53−55] and even lower than many conversion cathodes for LIBs.[56,57] SEM and EDS were employed to confirm that there is no transport of Mg sulfide to the Mg anode (Figure S3). Within the first three cycles, a reversible capacity of ~400 mA h/g is maintained, corresponding to a gravimetric energy density of 608 Wh/kg, which until now is the highest among all of the reported intercalation and conversion cathodes for RMBs.[4,6,7,9]

Long-term cycling performance of the CuS/Mg system was evaluated with a MACC electrolyte at 5 mA/g and RT (Figure 2b). The rapid loss of capacity for the first 10 cycles can be attributed to some $Mg^{2+}$ trapped in CuS, indicated by a low Coulombic efficiency (less than 99.4%). In addition, the dissolution of copper ions into electrolyte also leads to a



DOI: 10.1021/acs.nanolett.9b02963
*Nano Lett.* 2019, 19, 6665−6672

capacity loss (Cu concentration in cycled MACC electrolyte: 1.29 ppm according to ICP), which is common in copper-based cathodes.[57−60] The CuS/Mg full cells hold a capacity of ∼335 mA h/g after 80 cycles, which is much higher than that previously reported for CuS[46,47] and for the typical cathodes reported for RMBs (Table S1). It corresponds to a gravimetric energy density of ∼608 W h/kg, more than 4 times that of the Chevrel phase (140 W h/kg). More importantly, the volumetric energy density of the CuS/Mg pouch cell is 1042 W h/L (Table S2), which is much higher than for the conventional $LiCoO_2$/graphite pouch cell (491 W h/L).[1] In addition, the Coulombic efficiency (CE) reaches 98.1% in the 2nd cycle and remains steady at ∼99.6% after the 10th cycle, indicating the high reversibility of the CuS/Mg system. The CE of CuS is also much higher than that reported for CuS[46,47] because of the unique aggregated structure of CuS. To highlight the advantage of CuS microspheres, the electrochemical performance of commercial CuS (with an average diameter of ∼10 $\mu$m) (Figure S5) was also evaluated under the same testing conditions. The capacity of 26 mA h/g is delivered in the first discharge, whereas a negligible charging capacity (12 mA h/g) is achieved (Figure S6a). Very short voltage plateaus are presented with large polarization. No improvement in capacity occurs after 10 cycles (Figure S6b), which is in agreement with the results reported by Duffort et al. at RT and 60 °C.[46] It further validates the advantages of the microsized secondary particles with respect to kinetics.

To further demonstrate the merits of CuS secondary microspheres, higher current densities were applied (Figure 2c). Even at 50 (C/10) and 100 mA/g (C/5), CuS/Mg full cells still achieve high capacities of 260 and 190 mA h/g, respectively, which are much better than those reported for CuS cathodes,[47] corroborating the fast magnesiation kinetics of CuS. We also conservatively evaluated the volumetric energy density of the Mg pouch cell, according to Aurbach et al.,[1] if the capacity (400 mA h/g) of CuS at 1.52 V is taken into account (Table S2). By taking the material prices according to reports,[1,61,62] we estimated the unit cost required for the pouch cell and plotted the volumetric energy density versus the unit cost of LIBs, NIBs, and RMBs (Figure 2d). The energy density of 1042 W h/L for the CuS/Mg system is much higher than for current LIBs ($LiCoO_2$/graphite and $LiNi_{0.8}Co_{0.1}Mn_{0.1}O_2$/graphite) and near-term LIBs ($LiNi_{0.8}Co_{0.1}Mn_{0.1}O_2$/graphite-$SiO_x$) and even higher than for long-term LIBs (650 W h/L for Li-$Ni_{0.8}Co_{0.1}Mn_{0.1}O_2$/Li) with a much lower unit cost, which is mainly due to the abundance and low cost of Mg and CuS. The high energy density and low cost endow the CuS/Mg system with great promise as a candidate for LIBs in customer electronics.

To better understand the reaction kinetics of CuS during discharge and charge, the overpotential from quasi-equilibrium states was collected using the galvanostatic intermittent titration technique (GITT). GITT can provide both thermodynamic hysteresis and kinetic polarization.[63] The cells were allowed to relax at open circuit for 8 h to reach quasi-equilibrium, after each 2 h discharging or charging period at 5 mA/g in the first cycle (Figure 3a). The cumulative capacities are 536 mA h/g on discharging (280 and 256 mA h/g for the first and second voltage plateaus, respectively) and 515 mA h/g on charging, both of which are more than what has been achieved during galvanostatic discharging/charging. Apparently, during discharge, the overpotential in the first plateau is smaller than that in the second one, indicating faster reaction kinetics in the first plateau. The quasi-equilibrium potentials obtained from GITT are very close to the theoretical equilibrium potentials of 1.66 and 1.38 V vs $Mg/Mg^{2+}$ predicated using the first principles calculation (Figure 3b).[64] The deviation between calculated and measured potentials for the first plateau is 37 mV, which is comparable to that for the second plateau (39 mV).

The dynamic potential response after current cutoff during the GITT measurement was carefully analyzed as shown in Figure 3c. In the discharge process (black curve), once the current is removed, the voltage first jumps by a small value because of the charge transfer and ohm resistance (IR) and then gradually increases, corresponding to the removal of concentration polarization by ion diffusion ($\eta$) until it approaches the quasi-equilibrium conditions after 8 h of relaxation.[65] The opposite occurs in the charging process (red curve). The thermodynamic voltage hysteresis between the charge and discharge ($V_{gap}$) is rather small (∼0.05 V). The overpotential between with current on and after 8 h of relaxation for the discharging and charging process is shown in Figure 3d. The overpotential for the second discharge plateau is larger than that for the first one, which can be assigned to the lower diffusion coefficient and electronic conductivity of $Cu_2S$.[66−68] For both plateaus, the overpotential in the charging process is higher than that in discharging process, indicating more sluggish kinetics in demagnesiation than in magnesiation, also explaining why the charge capacity is smaller than the discharge capacity.

In addition to the quasi-equilibrium potential and overpotential, the chemical diffusion coefficient for $Mg^{2+}$ in CuS at different charge/discharge states can also be obtained from GITT using eq 1.[69,70]

$$D = \frac{4}{\pi}\left(\frac{IV_M}{Z_A FS}\right)^2 \left[\frac{\frac{dE(x)}{dx}}{\frac{dE(t)}{d\sqrt{t}}}\right]^2 \quad (1)$$

$I$ is the applied constant current, $V_M$ is the molar volume of CuS (20.09 $cm^3$/mol), assumed to be constant during the electrochemical process, $Z_A$ is the charge number of electroactive species $Mg^{2+}$, $F$ is the Faraday constant (96 486 C/mol), $S$ is the electrochemical active area between the electrode material and electrolyte from the Brunauer−Emmett−Teller (BET) surface area ($S_{BET}$ = 17 870 $cm^2$/g) (Figure S7a), $E(x)$ is the steady-state equilibrium voltage (i.e., open circuit voltage) of the working electrode (vs the reference electrode) at the composition of $Mg_xCuS$, and $E(t)$ is the transient voltage response of the working electrode during the constant current interval.

Equation 1 could be applied only in solid-solution materials,[69] not in the phase-transition regions, in which the value of $dE/dx$ should be zero according to the Gibbs phase rule. We calculated only the ion diffusion coefficient in the solid-solution region near the end of discharging and charging. The transient voltage versus the square root of the time was plotted in Figure 3e. Plugging the slope of the linear fitting into eq 1, we can get the diffusion coefficient of $Mg^{2+}$ in CuS for the first discharge plateau to be $1.97 \times 10^{-14}$ $cm^2$/s, which is higher than that of $LiFePO_4$ ($6.77 \times 10^{-16}$ $cm^2$/s).[70] Actually, the higher diffusion coefficient does not dictate a faster reaction because the magnesiation of CuS is a phase-transition reaction whose rate not only depends on the diffusion rate but also relies on the speed of the phase transition. Applying the same method, the diffusion coefficients for the second discharge plateau and charge plateau are $1.84 \times 10^{-15}$ and $6.83 \times 10^{-16}$ $cm^2$/s, respectively, consistent with the larger overpotential in the charging process. According to $t \approx L^2/D$ (in



DOI: 10.1021/acs.nanolett.9b02963
Nano Lett. 2019, 19, 6665−6672

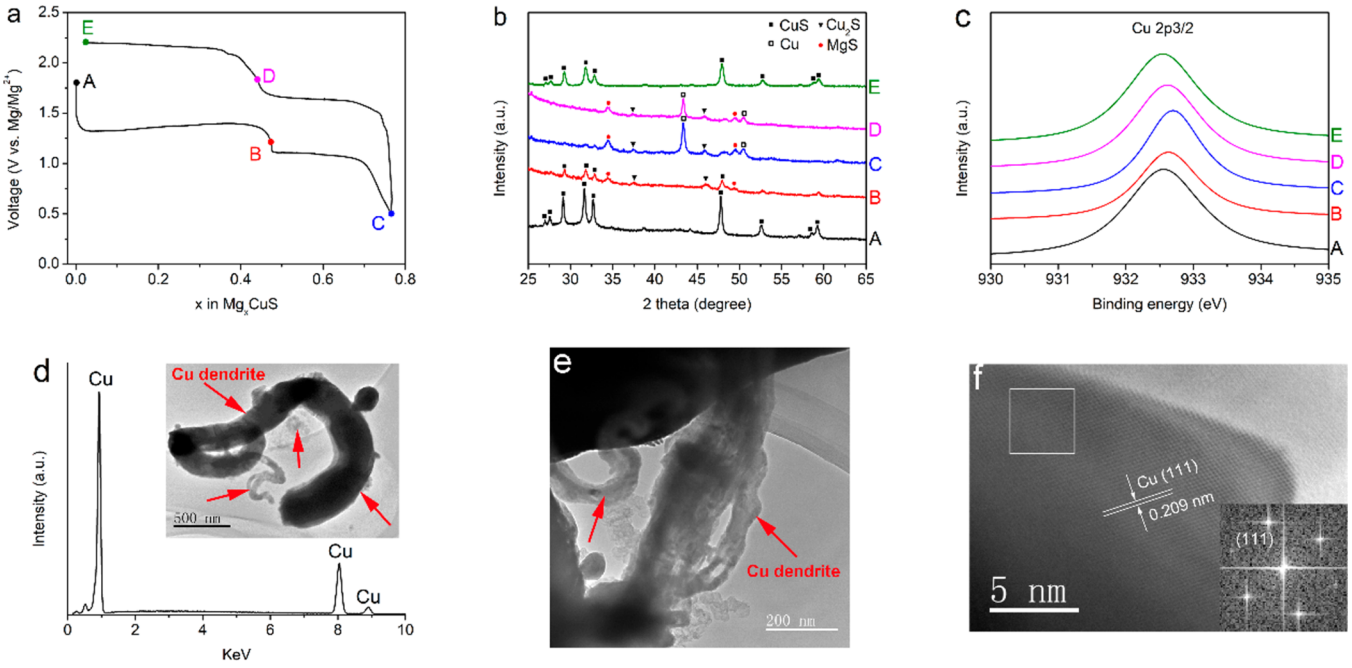


**Figure 4.** Studies on the reaction mechanism of CuS during cycling. (a) Electrochemical discharging−charging profile of the first cycle showing the labeling of the points at which diffraction patterns were collected. (A) Pristine CuS, (B) discharged to 1.2 V (end of the first discharge plateau), (C) fully discharged to 0.5 V, (D) recharged to 1.8 V (end of the first charge plateau), and (E) fully recharged to 2.2 V. The ex situ (b) XRD and (c) XPS Cu $2p_{3/2}$ of CuS in various states during the first cycle. (d, e) Bright-field TEM image and EDS recorded on the fully reduced MgCuS at 0.5 V showing a large copper dendrite (marked with arrows in red). (f) HRTEM and FFT of the copper dendrite.

which $t$ represents the diffusion time and $L$ represents the diffusion length), reducing the particle size will shorten the ionic diffusion path as well as the diffusion time, which is an effective method of improving the kinetics. It also explains why commercial CuS (~10 $\mu$m according to Figure S4) delivers only a negligible capacity in this paper and that by Duffort et al.,[46] whereas CuS secondary microspheres assembled by nanoparticles (~200 nm) achieve a high capacity.

The reaction mechanism of CuS with Mg was investigated by ex situ XRD, XPS, SEM, TEM, and EDS during the first cycle (Figures 4 and S8−S13). For ex situ XRD, during Mg insertion (discharge) (from A to B), $Cu_2S$ (PDF no. 26-1116) and MgS (PDF no. 65-0895) peaks emerge before 1.2 V, with the intensity of CuS drastically decreasing, indicating that reaction II occurs. However, because of sluggish kinetics, reaction II is not accomplished completely, leaving some CuS unreacted, which is consistent with the fact that the corresponding capacity (203 mA h/g) is less than the theoretical capacity of reaction II (280 mA h/g). Upon further discharge (from B to C), peaks for MgS are enhanced, with Cu peaks (PDF no. 65-9026) emerging and $Cu_2S$ peaks weakened, suggesting that reaction III proceeds. Also, reaction III is not completed, in accordance with the corresponding capacity of 227 mA h/g (81.1% of the theoretical capacity). Upon recharge (from C to D), MgS and Cu peaks gradually recede, indicating that reaction III proceeds in the inverse direction, with the charge capacity of 160 mA h/g being less than the discharge capacity on the second voltage plateau (227 mA h/g). When the CuS/Mg system is fully recharged to 2.2 V (from D to E), the final charged product is back to CuS. In the following discharge/charge cycles, reactions II and III proceed reversibly. The reaction equations are the following:

$$CuS + 0.5Mg^{2+} + e^- \leftrightarrow 0.5Cu_2S + 0.5MgS \quad \text{(II)}$$

$$0.5Cu_2S + 0.5Mg^{2+} + e^- \leftrightarrow Cu + 0.5MgS \quad \text{(III)}$$

The reaction mechanism is further confirmed by ex situ XPS (Figure 4c), in which the C 1s peak at 284.8 eV is used as a reference binding energy (Figure S8). During discharging from A to B, the binding energy increases from 932.55 to 932.62 eV, indicating that CuS is transformed to $Cu_2S$.[71,72] Upon further discharge to C (the fully discharged state), the binding energy of 932.71 eV represents the appearance of metallic copper,[73] which is the final product of the discharging process. In the following recharging process, the binding energies of 932.63 eV (at point D) and 932.54 eV (at point E) indicate the reformation of $Cu_2S$ and CuS, respectively. Therefore, the Mg insertion/extraction of CuS is highly reversible, which is consistent with the results of ex situ XRD. However, the oxidation state of sulfur does not change with the cycle (Figure S9), indicating that Cu is the only redox-active element in the magnesiation/demagnesiation of CuS. Energy-dispersive X-ray spectroscopy (EDS) was also conducted to investigate the magnesiation mechanism of CuS (Figure S10). Five electrodes on different discharge/charge states (from A to E) indicate that the amount of inserted Mg corresponds well to the specific capacity.

To thoroughly investigate the magnesiation mechanism of CuS, we re-examined the discharge−charge characterizations. Because the first discharge potential of a conversion reaction is always lower than that in the following discharging process, which is a typical characteristic of the conversion cathode, the absence of a voltage difference between the first and second discharging processes suggests that a displacement rather than a conversion reaction seems more likely (Figure 2a).[74] SEM, TEM, and EDS are applied to reveal the displacement reaction (Figures 4d−f and S11−S13). Fully discharged to 0.5 V, a large amount of Cu dendrite can be found in different-magnification SEM images, which is highlighted by red arrows (Figure S11), in



DOI: 10.1021/acs.nanolett.9b02963
Nano Lett. 2019, 19, 6665−6672

contrast to no Cu dendrite in other discharge/charge states (Figure S12). TEM images of an electrode discharged to 0.5 V clearly reveal that large Cu dendrites (several micrometers long) grow out toward the core particles (Figure 4d,e). EDS demonstrates that the dendrite is metallic copper (Figure 4d), which is further confirmed by HRTEM and FFT (Figure 4e).

The crystal structure of CuS and discharged product MgS is examined (Figure S14). The projected structure of CuS and MgS is drawn along the [001] and [110] directions, respectively, in which the sulfur atoms form in a layer stacking sequence. Between these sulfur layers, the copper and magnesium cations make zigzag chains and a straight line, respectively. When Mg ions are "inserted" into the CuS material, they "insert" between the sulfur layers and drive out copper cations with high mobility to form a metal copper dendrite, which undergoes a displacement reaction. It has been reported that Li insertion/extraction into CuS also occurs through displacement, providing 550 mA h/g (98% of its theoretical capacity).[60,75] Upon lithiation, the insertion of the guest cations ($Li^+$) will induce the displacement and extrusion of transition-metal cations ($Cu^{2+}$) from original sites, with $Cu^{2+}$ reduced to $Cu^0$, which might be isolated as a metal precipitate. Upon charging, $Cu^0$ is reoxidized to $Cu^{2+}$ and injected into the host structure, replacing the $Li^+$ in the discharged products.[74] The high Cu mobility via a vacancy mechanism is the key to achieving the displacement,[66,76] which will contribute to the improved kinetics of cathode materials. The fast displacement kinetics of CuS with Mg enables fast Mg diffusion and high occupancy in the crystal. Even so, the large charge/radius ratio of $Mg^{2+}$ results in strong interaction between $Mg^{2+}$ with CuS and slower reaction kinetics of CuS in RMBs compared to that in LIBs.[74]

We, for the first time, demonstrated the fully reversible CuS cathode through a displacement reaction in CuS/Mg pouch cells at RT, which delivers a reversible capacity of ~400 mA h/g for the first three cycles between 0.5 and 2.2 V, corresponding to a volumetric density of 1042 W h/L, which is much higher than for $LiCoO_2$-graphite (491 W h/L). A capacity of 335 mA h/g is maintained after 80 cycles. At higher current densities of 50 (C/10) and 100 mA/g (C/5), CuS/Mg full cells still achieve capacities of 260 and 190 mA h/g, respectively, indicating the fast magnesiation kinetics. Two-step reactions with two equilibrium potential plateaus obtained from GITT are validated by the first principles calculation, and the fast reaction kinetics of CuS is also demonstrated by the high diffusivity of $Mg^{2+}$ in CuS and a low overpotential of less than 0.4 V. The fast reaction kinetics of CuS with $Mg^{2+}$ is attributed to the displacement reaction mechanism, as evidenced by ex situ XRD, XPS, SEM, TEM, and almost identical discharge curves in the first and the second cycles. This displacement reaction can greatly improve the kinetics of cathodes and enable stable cycling performance, which provides a direction for finding feasible cathodes for RMBs. The optimization of the Mg anode and electrolyte is also needed to improve the kinetics of the Mg anode. We believe this work will provide a guide for more discovery of high-performance cathode candidates for RMBs at RT.

## ■ ASSOCIATED CONTENT

### Supporting Information

The Supporting Information is available free of charge on the ACS Publications website at DOI: 10.1021/acs.nanolett.9b02963.

Detailed description of the experiment, including the preparation of cathode materials and electrode sheets, cell fabrication, and performance evaluation; supporting figures, including SEM images of CuS, BET, XPS spectra, EDS mapping, TEM images, and electrochemical performance (PDF)

## ■ AUTHOR INFORMATION


### Corresponding Author

*E-mail: cswang@umd.edu.

### ORCID

Tao Gao: 0000-0003-0204-3269

Ji Chen: 0000-0003-0326-8304

Xiulin Fan: 0000-0001-7294-480X

Chunsheng Wang: 0000-0002-8626-6381

### Author Contributions

§These authors contributed equally to this work.


### Notes

The authors declare no competing financial interest.

## ■ ACKNOWLEDGMENTS

The authors thank Miss Yuxin Tong and Jinming Yue from the Institute of Physics, Chinese Academy of Sciences for help with TEM and XPS, respectively. The authors acknowledge the support from the Army Research Office (grant no. W911NF-15-1-0187) and Nanostructures for Electrical Energy Storage (NEES), an Energy Frontier Research Center funded by the U.S. Department of Energy, Office of Science, Basic Energy Sciences, under award no. DESC0001160. This work was also supported by the National Natural Science Foundation of China (grant no. 21905299), the Hunan Provincial Innovation Foundation for Postgraduate (no. CX2016B120). M.M.'s fellowship was supported by the China Scholarship Council (grant no. 201606130050). This work was also supported by the China Postdoctoral Science Foundation (2019TQ0346).

## ■ REFERENCES


(1) Choi, J. W.; Aurbach, D. Promise and reality of post-lithium-ion batteries with high energy densities. *Nature Reviews Materials* **2016**, *1*, 16013.

(2) Etacheri, V.; Marom, R.; Elazari, R.; Salitra, G.; Aurbach, D. Challenges in the development of advanced Li-ion batteries: a review. *Energy Environ. Sci.* **2011**, *4* (9), 3243−3262.

(3) Whittingham, M. S. Ultimate Limits to Intercalation Reactions for Lithium Batteries. *Chem. Rev.* **2014**, *114* (23), 11414−11443.

(4) Muldoon, J.; Bucur, C. B.; Gregory, T. Quest for Nonaqueous Multivalent Secondary Batteries: Magnesium and Beyond. *Chem. Rev.* **2014**, *114* (23), 11683−11720.

(5) Yoo, H. D.; Shterenberg, I.; Gofer, Y.; Gershinsky, G.; Pour, N.; Aurbach, D. Mg rechargeable batteries: an on-going challenge. *Energy Environ. Sci.* **2013**, *6* (8), 2265−2279.

(6) Mao, M.; Gao, T.; Hou, S.; Wang, C. A critical review of cathodes for rechargeable Mg batteries. *Chem. Soc. Rev.* **2018**, *47* (23), 8804−8841.

(7) Canepa, P.; Sai Gautam, G.; Hannah, D. C.; Malik, R.; Liu, M.; Gallagher, K. G.; Persson, K. A.; Ceder, G. Odyssey of Multivalent Cathode Materials: Open Questions and Future Challenges. *Chem. Rev.* **2017**, *117* (5), 4287−4341.

(8) Huie, M. M.; Bock, D. C.; Takeuchi, E. S.; Marschilok, A. C.; Takeuchi, K. J. Cathode materials for magnesium and magnesium-ion based batteries. *Coord. Chem. Rev.* **2015**, *287*, 15−27.

(9) Shterenberg, I.; Salama, M.; Gofer, Y.; Levi, E.; Aurbach, D. The challenge of developing rechargeable magnesium batteries. *MRS Bull.* **2014**, *39* (5), 453−460.




DOI: 10.1021/acs.nanolett.9b02963
*Nano Lett.* 2019, 19, 6665−6672

(10) Matsui, M. Study on electrochemically deposited Mg metal. *J. Power Sources* **2011**, *196* (16), 7048−7055.
(11) Ling, C.; Banerjee, D.; Matsui, M. Study of the electrochemical deposition of Mg in the atomic level: Why it prefers the non-dendritic morphology. *Electrochim. Acta* **2012**, *76*, 270−274.
(12) Mizrahi, O.; Amir, N.; Pollak, E.; Chusid, O.; Marks, V.; Gottlieb, H.; Larush, L.; Zinigrad, E.; Aurbach, D. Electrolyte Solutions with a Wide Electrochemical Window for Rechargeable Magnesium Batteries. *J. Electrochem. Soc.* **2008**, *155* (2), A103−A109.
(13) Zhamu, A.; Chen, G.; Liu, C.; Neff, D.; Fang, Q.; Yu, Z.; Xiong, W.; Wang, Y.; Wang, X.; Jang, B. Z. Reviving rechargeable lithium metal batteries: enabling next-generation high-energy and high-power cells. *Energy Environ. Sci.* **2012**, *5* (2), 5701−5707.
(14) Yoshimatsu, I.; Hirai, T.; Yamaki, J. i. Lithium Electrode Morphology during Cycling in Lithium Cells. *J. Electrochem. Soc.* **1988**, *135* (10), 2422−2427.
(15) Aurbach, D.; Gizbar, H.; Schechter, A.; Chusid, O.; Gottlieb, H. E.; Gofer, Y.; Goldberg, I. Electrolyte Solutions for Rechargeable Magnesium Batteries Based on Organomagnesium Chloroaluminate Complexes. *J. Electrochem. Soc.* **2002**, *149* (2), A115−A121.
(16) Aurbach, D.; Suresh, G. S.; Levi, E.; Mitelman, A.; Mizrahi, O.; Chusid, O.; Brunelli, M. Progress in Rechargeable Magnesium Battery Technology. *Adv. Mater.* **2007**, *19* (23), 4260−4267.
(17) Canepa, P.; Jayaraman, S.; Cheng, L.; Rajput, N. N.; Richards, W. D.; Gautam, G. S.; Curtiss, L. A.; Persson, K. A.; Ceder, G. Elucidating the structure of the magnesium aluminum chloride complex electrolyte for magnesium-ion batteries. *Energy Environ. Sci.* **2015**, *8* (12), 3718−3730.
(18) Doe, R. E.; Han, R.; Hwang, J.; Gmitter, A. J.; Shterenberg, I.; Yoo, H. D.; Pour, N.; Aurbach, D. Novel, electrolyte solutions comprising fully inorganic salts with high anodic stability for rechargeable magnesium batteries. *Chem. Commun.* **2014**, *50* (2), 243−245.
(19) See, K. A.; Chapman, K. W.; Zhu, L.; Wiaderek, K. M.; Borkiewicz, O. J.; Barile, C. J.; Chupas, P. J.; Gewirth, A. A. The Interplay of Al and Mg Speciation in Advanced Mg Battery Electrolyte Solutions. *J. Am. Chem. Soc.* **2016**, *138* (1), 328−337.
(20) Liu, M.; Jain, A.; Rong, Z.; Qu, X.; Canepa, P.; Malik, R.; Ceder, G.; Persson, K. A. Evaluation of sulfur spinel compounds for multivalent battery cathode applications. *Energy Environ. Sci.* **2016**, *9* (10), 3201−3209.
(21) Aurbach, D.; Lu, Z.; Schechter, A.; Gofer, Y.; Gizbar, H.; Turgeman, R.; Cohen, Y.; Moshkovich, M.; Levi, E. Prototype systems for rechargeable magnesium batteries. *Nature* **2000**, *407*, 724.
(22) Rong, Z.; Malik, R.; Canepa, P.; Sai Gautam, G.; Liu, M.; Jain, A.; Persson, K.; Ceder, G. Materials Design Rules for Multivalent Ion Mobility in Intercalation Structures. *Chem. Mater.* **2015**, *27* (17), 6016−6021.
(23) Liu, M.; Rong, Z.; Malik, R.; Canepa, P.; Jain, A.; Ceder, G.; Persson, K. A. Spinel compounds as multivalent battery cathodes: a systematic evaluation based on ab initio calculations. *Energy Environ. Sci.* **2015**, *8* (3), 964−974.
(24) Kim, C.; Phillips, P. J.; Key, B.; Yi, T.; Nordlund, D.; Yu, Y.-S.; Bayliss, R. D.; Han, S.-D.; He, M.; Zhang, Z.; Burrell, A. K.; Klie, R. F.; Cabana, J. Direct Observation of Reversible Magnesium Ion Intercalation into a Spinel Oxide Host. *Adv. Mater.* **2015**, *27* (22), 3377−3384.
(25) Feng, Z.; Chen, X.; Qiao, L.; Lipson, A. L.; Fister, T. T.; Zeng, L.; Kim, C.; Yi, T.; Sa, N.; Proffit, D. L.; Burrell, A. K.; Cabana, J.; Ingram, B. J.; Biegalski, M. D.; Bedzyk, M. J.; Fenter, P. Phase-Controlled Electrochemical Activity of Epitaxial Mg-Spinel Thin Films. *ACS Appl. Mater. Interfaces* **2015**, *7* (51), 28438−28443.
(26) Cabello, M.; Alcántara, R.; Nacimiento, F.; Ortiz, G.; Lavela, P.; Tirado, J. L. Electrochemical and chemical insertion/deinsertion of magnesium in spinel-type MgMn2O4 and lambda-MnO2 for both aqueous and non-aqueous magnesium-ion batteries. *CrystEngComm* **2015**, *17* (45), 8728−8735.
(27) Sun, X.; Bonnick, P.; Duffort, V.; Liu, M.; Rong, Z.; Persson, K. A.; Ceder, G.; Nazar, L. F. A high capacity thiospinel cathode for Mg batteries. *Energy Environ. Sci.* **2016**, *9* (7), 2273−2277.
(28) Emly, A.; Van der Ven, A. Mg Intercalation in Layered and Spinel Host Crystal Structures for Mg Batteries. *Inorg. Chem.* **2015**, *54* (9), 4394−4402.
(29) Sun, X.; Bonnick, P.; Nazar, L. F. Layered TiS2 Positive Electrode for Mg Batteries. *ACS Energy Letters* **2016**, *1* (1), 297−301.
(30) Gu, Y.; Katsura, Y.; Yoshino, T.; Takagi, H.; Taniguchi, K. Rechargeable magnesium-ion battery based on a TiSe2-cathode with d-p orbital hybridized electronic structure. *Sci. Rep.* **2015**, *5*, 12486.
(31) Gautam, G. S.; Canepa, P.; Malik, R.; Liu, M.; Persson, K.; Ceder, G. First-principles evaluation of multi-valent cation insertion into orthorhombic V2O5. *Chem. Commun.* **2015**, *51* (71), 13619−13622.
(32) Mao, M.; Ji, X.; Hou, S.; Gao, T.; Wang, F.; Chen, L.; Fan, X.; Chen, J.; Ma, J.; Wang, C. Tuning Anionic Chemistry To Improve Kinetics of Mg Intercalation. *Chem. Mater.* **2019**, *31* (9), 3183−3191.
(33) Ling, C.; Banerjee, D.; Song, W.; Zhang, M.; Matsui, M. First-principles study of the magnesiation of olivines: redox reaction mechanism, electrochemical and thermodynamic properties. *J. Mater. Chem.* **2012**, *22* (27), 13517−13523.
(34) Zhang, R.; Ling, C. Unveil the Chemistry of Olivine FePO4 as Magnesium Battery Cathode. *ACS Appl. Mater. Interfaces* **2016**, *8* (28), 18018−18026.
(35) Orikasa, Y.; Masese, T.; Koyama, Y.; Mori, T.; Hattori, M.; Yamamoto, K.; Okado, T.; Huang, Z.-D.; Minato, T.; Tassel, C.; Kim, J.; Kobayashi, Y.; Abe, T.; Kageyama, H.; Uchimoto, Y. High energy density rechargeable magnesium battery using earth-abundant and non-toxic elements. *Sci. Rep.* **2015**, *4*, 5622.
(36) Tian, H.; Gao, T.; Li, X.; Wang, X.; Luo, C.; Fan, X.; Yang, C.; Suo, L.; Ma, Z.; Han, W.; Wang, C. High power rechargeable magnesium/iodine battery chemistry. *Nat. Commun.* **2017**, *8*, 14083.
(37) Vardar, G.; Nelson, E. G.; Smith, J. G.; Naruse, J.; Hiramatsu, H.; Bartlett, B. M.; Sleightholme, A. E. S.; Siegel, D. J.; Monroe, C. W. Identifying the Discharge Product and Reaction Pathway for a Secondary Mg/O2 Battery. *Chem. Mater.* **2015**, *27* (22), 7564−7568.
(38) Smith, J. G.; Naruse, J.; Hiramatsu, H.; Siegel, D. J. Theoretical Limiting Potentials in Mg/O2 Batteries. *Chem. Mater.* **2016**, *28* (5), 1390−1401.
(39) Vardar, G.; Smith, J. G.; Thompson, T.; Inagaki, K.; Naruse, J.; Hiramatsu, H.; Sleightholme, A. E. S.; Sakamoto, J.; Siegel, D. J.; Monroe, C. W. Mg/O2 Battery Based on the Magnesium−Aluminum Chloride Complex (MACC) Electrolyte. *Chem. Mater.* **2016**, *28* (21), 7629−7637.
(40) Zhao-Karger, Z.; Zhao, X.; Wang, D.; Diemant, T.; Behm, R. J.; Fichtner, M. Performance Improvement of Magnesium Sulfur Batteries with Modified. *Non-Nucleophilic Electrolytes* **2015**, *5* (3), 1401155.
(41) Gao, T.; Hou, S.; Wang, F.; Ma, Z.; Li, X.; Xu, K.; Wang, C. Reversible S0/MgSx Redox Chemistry in a MgTFSI2/MgCl2/DME Electrolyte for Rechargeable Mg/S Batteries. *Angew. Chem.* **2017**, *129* (43), 13711−13715.
(42) Gao, T.; Ji, X.; Hou, S.; Fan, X.; Li, X.; Yang, C.; Han, F.; Wang, F.; Jiang, J.; Xu, K.; Wang, C. Thermodynamics and Kinetics of Sulfur Cathode during Discharge in MgTFSI2−DME Electrolyte. *Adv. Mater.* **2018**, *30* (3), 1704313.
(43) Gao, T.; Hou, S.; Huynh, K.; Wang, F.; Eidson, N.; Fan, X.; Han, F.; Luo, C.; Mao, M.; Li, X.; Wang, C. Existence of Solid Electrolyte Interphase in Mg Batteries: Mg/S Chemistry as an Example. *ACS Appl. Mater. Interfaces* **2018**, *10* (17), 14767−14776.
(44) Sun, K.; Su, D.; Zhang, Q.; Bock, D. C.; Marschilok, A. C.; Takeuchi, K. J.; Takeuchi, E. S.; Gan, H. Interaction of CuS and Sulfur in Li-S Battery System. *J. Electrochem. Soc.* **2015**, *162* (14), A2834−A2839.
(45) He, K.; Yao, Z.; Hwang, S.; Li, N.; Sun, K.; Gan, H.; Du, Y.; Zhang, H.; Wolverton, C.; Su, D. Kinetically-Driven Phase Transformation during Lithiation in Copper Sulfide Nanoflakes. *Nano Lett.* **2017**, *17* (9), 5726−5733.


DOI: 10.1021/acs.nanolett.9b02963
*Nano Lett.* 2019, 19, 6665−6672

(46) Duffort, V.; Sun, X.; Nazar, L. F. Screening for positive electrodes for magnesium batteries: a protocol for studies at elevated temperatures. *Chem. Commun.* **2016**, *52* (84), 12458−12461.
(47) Xiong, F.; Fan, Y.; Tan, S.; Zhou, L.; Xu, Y.; Pei, C.; An, Q.; Mai, L. Magnesium storage performance and mechanism of CuS cathode. *Nano Energy* **2018**, *47*, 210−216.
(48) Wang, F.; Robert, R.; Chernova, N. A.; Pereira, N.; Omenya, F.; Badway, F.; Hua, X.; Ruotolo, M.; Zhang, R.; Wu, L.; Volkov, V.; Su, D.; Key, B.; Whittingham, M. S.; Grey, C. P.; Amatucci, G. G.; Zhu, Y.; Graetz, J. Conversion Reaction Mechanisms in Lithium Ion Batteries: Study of the Binary Metal Fluoride Electrodes. *J. Am. Chem. Soc.* **2011**, *133* (46), 18828−18836.
(49) Malini, R.; Uma, U.; Sheela, T.; Ganesan, M.; Renganathan, N. G. J. I. Conversion reactions: a new pathway to realise energy in lithium-ion battery—review. *Ionics* **2009**, *15* (3), 301−307.
(50) Zhang, Y. C.; Hu, X. Y.; Qiao, T. Shape-controlled synthesis of CuS nanocrystallites via a facile hydrothermal route. *Solid State Commun.* **2004**, *132* (11), 779−782.
(51) Delacourt, C.; Poizot, P.; Levasseur, S.; Masquelier, C. Size Effects on Carbon-Free LiFePO4 Powders: The Key to Superior Energy Density. *Electrochem. Solid-State Lett.* **2006**, *9* (7), A352−A355.
(52) Ferrari, S.; Lavall, R. L.; Capsoni, D.; Quartarone, E.; Magistris, A.; Mustarelli, P.; Canton, P. Influence of Particle Size and Crystal Orientation on the Electrochemical Behavior of Carbon-Coated LiFePO4. *J. Phys. Chem. C* **2010**, *114* (29), 12598−12603.
(53) Gershinsky, G.; Yoo, H. D.; Gofer, Y.; Aurbach, D. Electrochemical and Spectroscopic Analysis of Mg2+ Intercalation into Thin Film Electrodes of Layered Oxides: V2O5 and MoO3. *Langmuir* **2013**, *29* (34), 10964−10972.
(54) Mukherjee, A.; Sa, N.; Phillips, P. J.; Burrell, A.; Vaughey, J.; Klie, R. F. Direct Investigation of Mg Intercalation into the Orthorhombic V2O5 Cathode Using Atomic-Resolution Transmission Electron Microscopy. *Chem. Mater.* **2017**, *29* (5), 2218−2226.
(55) Sa, N.; Kinnibrugh, T. L.; Wang, H.; Sai Gautam, G.; Chapman, K. W.; Vaughey, J. T.; Key, B.; Fister, T. T.; Freeland, J. W.; Proffit, D. L.; Chupas, P. J.; Ceder, G.; Bareno, J. G.; Bloom, I. D.; Burrell, A. K. Structural Evolution of Reversible Mg Insertion into a Bilayer Structure of V2O5·nH2O Xerogel Material. *Chem. Mater.* **2016**, *28* (9), 2962−2969.
(56) Li, T.; Li, L.; Cao, Y. L.; Ai, X. P.; Yang, H. X. Reversible Three-Electron Redox Behaviors of FeF3 Nanocrystals as High-Capacity Cathode-Active Materials for Li-Ion Batteries. *J. Phys. Chem. C* **2010**, *114* (7), 3190−3195.
(57) Hua, X.; Robert, R.; Du, L.-S.; Wiaderek, K. M.; Leskes, M.; Chapman, K. W.; Chupas, P. J.; Grey, C. P. Comprehensive Study of the CuF2 Conversion Reaction Mechanism in a Lithium Ion Battery. *J. Phys. Chem. C* **2014**, *118* (28), 15169−15184.
(58) Kalimuldina, G.; Taniguchi, I. Electrochemical properties of stoichiometric CuS coated on carbon fiber paper and Cu foil current collectors as cathode material for lithium batteries. *J. Mater. Chem. A* **2017**, *5* (15), 6937−6946.
(59) Dobashi, S.; Nakanishi, K.; Tanida, H.; Hashizaki, K.; Uchimoto, Y.; Hirai, T.; Yamaki, J.-i.; Ogumi, Z. Communication—XAFS Analysis of Discharge/Charge Reactions on the Li/CuCl2 Battery Cathode with LiPF6/Methyl. *J. Electrochem. Soc.* **2016**, *163* (5), A727−A729.
(60) Jache, B.; Mogwitz, B.; Klein, F.; Adelhelm, P. Copper sulfides for rechargeable lithium batteries: Linking cycling stability to electrolyte composition. *J. Power Sources* **2014**, *247*, 703−711.
(61) Berckmans, G.; Messagie, M.; Smekens, J.; Omar, N.; Vanhaverbeke, L.; Van Mierlo, J. Cost Projection of State of the Art Lithium-Ion Batteries for Electric Vehicles Up to 2030. *Energies* **2017**, *10* (9), 1314.
(62) Blomgren, G. E. The Development and Future of Lithium Ion Batteries. *J. Electrochem. Soc.* **2017**, *164* (1), A5019−A5025.
(63) Fan, X.; Hu, E.; Ji, X.; Zhu, Y.; Han, F.; Hwang, S.; Liu, J.; Bak, S.; Ma, Z.; Gao, T.; Liou, S.-C.; Bai, J.; Yang, X.-Q.; Mo, Y.; Xu, K.; Su, D.; Wang, C. High energy-density and reversibility of iron fluoride cathode enabled via an intercalation-extrusion reaction. *Nat. Commun.* **2018**, *9* (1), 2324.
(64) Chase, M. W., Jr. *NIST-JANAF Thermochemical Tables*, 4th ed.; Journal of Physical and Chemical Reference Data. Monograph; no. 9; American Institute of Physics for the National Institute of Standards and Technology: Woodbury, NY, 1998.
(65) Weppner, W.; Huggins, R. A. Determination of the Kinetic Parameters of Mixed-Conducting Electrodes and Application to the System Li3Sb. *J. Electrochem. Soc.* **1977**, *124* (10), 1569−1578.
(66) Cassaignon, S.; Sanchez, S.; Guillemoles, J. F.; Vedel, J.; Meier, H. G. Influence of the Composition on the Copper Diffusion in Copper Sulfides Study by Impedance Spectroscopy. *J. Electrochem. Soc.* **1999**, *146* (12), 4666−4671.
(67) Cassaignon, S.; Pauporté, T.; Guillemoles, J.-F.; Vedel, J. J. I. Copper diffusion in copper sulfide: a systematic study. *Ionics* **1998**, *4* (5), 364−371.
(68) Etienne, A. Electrochemical Method to Measure the Copper Ionic Diffusivity in a Copper Sulfide Scale. *J. Electrochem. Soc.* **1970**, *117* (7), 870−874.
(69) Wen, C. J.; Boukamp, B. A.; Huggins, R. A.; Weppner, W. Thermodynamic and Mass Transport Properties of "LiAl". *J. Electrochem. Soc.* **1979**, *126* (12), 2258−2266.
(70) Zhu, Y.; Xu, Y.; Liu, Y.; Luo, C.; Wang, C. Comparison of electrochemical performances of olivine NaFePO4 in sodium-ion batteries and olivine LiFePO4 in lithium-ion batteries. *Nanoscale* **2013**, *5* (2), 780−787.
(71) Perry, D. L.; Taylor, J. A. X-ray photoelectron and Auger spectroscopic studies of Cu2S and CuS. *J. Mater. Sci. Lett.* **1986**, *5* (4), 384−386.
(72) Nakai, I.; Sugitani, Y.; Nagashima, K.; Niwa, Y. X-ray photoelectron spectroscopic study of copper minerals. *J. Inorg. Nucl. Chem.* **1978**, *40* (5), 789−791.
(73) Folmer, J. C. W.; Jellinek, F. The valence of copper in sulphides and selenides: An X-ray photoelectron spectroscopy study. *J. Less-Common Met.* **1980**, *76* (1), 153−162.
(74) Débart, A.; Dupont, L.; Patrice, R.; Tarascon, J. M. Reactivity of transition metal (Co, Ni, Cu) sulphides versus lithium: The intriguing case of the copper sulphide. *Solid State Sci.* **2006**, *8* (6), 640−651.
(75) Chung, J. S.; Sohn, H. J. Electrochemical behaviors of CuS as a cathode material for lithium secondary batteries. *J. Power Sources* **2002**, *108* (1), 226−231.
(76) Morcrette, M.; Rozier, P.; Dupont, L.; Mugnier, E.; Sannier, L.; Galy, J.; Tarascon, J. M. A reversible copper extrusion−insertion electrode for rechargeable Li batteries. *Nat. Mater.* **2003**, *2*, 755.



DOI: 10.1021/acs.nanolett.9b02963
*Nano Lett.* 2019, 19, 6665−6672